Received: 6 October 2022 | Revised: 20 December 2022 | Accepted: 5 January 2023

DOI: 10.1096/fj.202201614R

THE FASEB JOURNAL

RESEARCH ARTICLE

Targeted deletion of *Fgf9* in tendon disrupts mineralization of the developing enthesis

Elahe Ganji[1,2,3,4] | **Connor Leek**[1,4] | **William Duncan**[4] | **Debabrata Patra**[5] | **David M. Ornitz**[5] | **Megan L. Killian**[1,4]

[1]Department of Orthopaedic Surgery, Michigan Medicine, Michigan, Ann Arbor, USA

[2]Department of Mechanical Engineering, University of Delaware, Delaware, Newark, USA

[3]Beckman Institute for Advanced Science and Technology, University of Illinois at Urbana-Champaign, 61801, IL, Urbana, United States

[4]Department of Biomedical Engineering, University of Delaware, Delaware, Newark, USA

[5]Department of Developmental Biology, Washington University School of Medicine, Missouri, St Louis, USA

Correspondence
Megan L. Killian, Department of Orthopaedic Surgery, Michigan Medicine, 109 Zina Pitcher Place, Ann Arbor, MI 48109, USA.
Email: mlkillia@med.umich.edu

Funding information
National Institutes of Health, Grant/Award Number: R01AR079367, R03HD094594, K12HD073945, P30GM103333, P30AR069620, R01AR079246 and R01HD049808; National Science Foundation, Grant/Award Number: 16A01396

Abstract

The enthesis is a transitional tissue between tendon and bone that matures postnatally. The development and maturation of the enthesis involve cellular processes likened to an arrested growth plate. In this study, we explored the role of fibroblast growth factor 9 (*Fgf9*), a known regulator of chondrogenesis and vascularization during bone development, on the structure and function of the postnatal enthesis. First, we confirmed spatial expression of *Fgf9* in the tendon and enthesis using in situ hybridization. We then used Cre-lox recombinase to conditionally knockout *Fgf9* in mouse tendon and enthesis (*Scx-Cre*) and characterized enthesis morphology as well as mechanical properties in $Fgf9^{ScxCre}$ and wild-type (WT) entheses. $Fgf9^{ScxCre}$ mice had smaller calcaneal and humeral apophyses, thinner cortical bone at the attachment, increased cellularity, and reduced failure load in mature entheses compared to WT littermates. During postnatal development, we found reduced chondrocyte hypertrophy and disrupted type X collagen (Col X) in $Fgf9^{ScxCre}$ entheses. These findings support that tendon-derived *Fgf9* is important for functional development of the enthesis, including its postnatal mineralization. Our findings suggest the potential role of FGF signaling during enthesis development.

KEYWORDS
attachment, enthesis, fibroblast growth factor, musculoskeletal, postnatal, tendon

Abbreviations: BMD, bone mineral density; BV, bone volume; Col X, type X collagen; CSA, cross sectional area; ECM, extracellular matrix; FGF, fibroblast growth factor; FGFR, fibroblast growth factor receptor; H&E, Hematoxylin and Eosin Y; MPa, megaPascals; P, Postnatal day; Scx, Scleraxis; SOC, secondary ossification center; TMD, Tissue mineral density; TV, total volume; WT, Wildtype.

1 | INTRODUCTION

The tendon-bone attachment (enthesis) is critical for the transmission of muscle-generated loads to the vertebrate skeleton. The enthesis forms embryonically as a compliant anchorage between tendon and bone.[1,2] The fibrocartilage enthesis matures postnatally into a graded transitional tissue with increasing mineral and proteoglycan content that reinforces the fibrous tendon into mineralized bone,[3] and its morphology mimics that of an arrested growth plate.[4,5] Growth plates of long bones and fibrocartilage entheses form primarily via endochondral ossification. Additionally, the cellular patterns of the developing enthesis form from a pool of progenitor cells that express *Sox9*, which is also a major regulator of the growth plate in long bones. However, the development of these two structures is not identical, as the growth plate fuses with age yet the enthesis remains fibrocartilaginous throughout the lifespan. In addition, the *Sox9*+ progenitor cells that establish the enthesis also co-express *Scleraxis*, which is not expressed in the growth plate.[6,7] Therefore, a gap in knowledge exists in identifying the similar and divergent patterns of the developing enthesis and growth plate during postnatal growth.

Recent studies by our laboratory and others have identified the potential role of fibroblast growth factors (*FGFs*) in the formation and adaptation of the entheses.[8,9] Several FGF ligands and their binding receptors (FGFR) are critical for growth plate development.[10–14] Specifically, FGF18 regulates chondrocyte proliferation and differentiation of the growth plate during bone development.[14] FGF9, together with FGF2 and 18, can compensate for each other during bone growth.[11,15–17] Spatially, FGF9 is most prevalent in the perichondrium and periosteum[18] and *Fgf9* expression regulates chondrocyte proliferation and hypertrophy through its affinity to FGFR3.[18] We and others have shown that global deletion of *Fgf9* during embryonic bone development results in reduced chondrocyte proliferation, delayed hypertrophy, and limb shortening in mouse embryos.[8,11,15] Global deletion of *Fgf9* in mouse embryos also leads to enlarged tuberosities, which are sites of tendon entheses.[8] Despite its prominent role in bone growth, the role of *Fgf9* during enthesis development remains unknown.

In this study, we aimed to identify the role of Fgf9 in *Scx*-lineage cells, as Scx is an early marker of the tendon/ligament progenitors, and its expression is essential for the formation and postnatal growth of the enthesis.[19–23] *Scx*-positive chondroprogenitors also contribute to chondrocyte differentiation at the bony eminence of the enthesis.[24,25] We generated mice to conditional knockout Fgf9 in Scx-lineage cells (using ScxCre) to study the structural and functional role of Fgf9 on the postnatal development of the fibrocartilage enthesis. We compared the mineral and cellular morphology as well as functional (mechanical) properties of the mature fibrocartilage entheses for both Achilles and supraspinatus attachments between normally developing (wildtype) and $Fgf9^{ScxCre}$ mice. We hypothesized that $Fgf9^{ScxCre}$ mice would develop disruptions in postnatal mineralization and organization of the mature fibrocartilaginous enthesis with impaired mechanical properties and reduced mineral content in the apophysis compared to normally developing littermates.

2 | MATERIALS AND METHODS

2.1 | Animal models

This study was approved by the Institutional Animal Care and Use Committees (IACUC) at the University of Delaware and the University of Michigan ($N = 52$ mice total). Mice were housed in 12 h on/off light cycle housing and placed in same-sex cages with littermates after weaning. Food and water were provided for ad libitum. To generate conditional knockout ($Fgf9^{ScxCre}$) mice, we crossed $Fgf9^{flx/+}$; ScxCre females with $Fgf9^{flx/flx}$ males. Offspring were genotyped using PCR (Transnetyx, Cordova, TN). Both male and female ScxCre; $Fgf9^{flx/flx}$ ($Fgf9^{ScxCre}$) and wildtype (WT; $Fgf9^{flx/flx}$) littermates were euthanized at 3 weeks (Young; $n = 7$/genotype) and 8 weeks (Adult; $n = 8$ $Fgf9^{ScxCre}$ and $n = 10$ WT) of age using carbon dioxide asphyxiation and thoracotomy. Both male and female mice were used, and a minimum of $n = 3$ per sex were collected for each time point and assay. Normal development of the fibrocartilage enthesis (i.e., Achilles' attachment) was assessed using an additional group of male WT mice at the following time points: Developing (postnatal day, P7-10, $n = 4$), Young adult (P15-28, $n = 7$), and Adult (P45-129, $n = 6$). A third cohort of WT mice ($n = 3$) was used for in situ hybridization at P0. Both hindlimbs and forelimbs were dissected at the time of euthanasia for imaging and contralateral hindlimbs were kept intact and stored at 4°C for uniaxial tensile testing.

2.2 | In situ hybridization

Spatial expression of *Fgf9* was visualized in the neonatal tendon enthesis using in situ hybridization (RNAscope Multiplex Fluorescent Reagent Kit v2, Advanced Cell Diagnostics, Hayward, CA, USA). P0 hindlimbs were decalcified in 14% EDTA for 2 weeks, paraffin-embedded, and sectioned at 7 μm thickness. Sections were labeled with mm*Fgf9* probe and both positive controls (probes targeting housekeeping genes *Polr2A, Ppib*, and *Ubc*)

and negative controls (*dapB*) were used. Nuclei were counterstained with DAPI and sections were mounted with Citifluor Antifade mounting medium (Electron Microscopy Science, Hatfield, PA, USA). Slides were imaged at 40X magnification using a fluorescent microscope (Lionheart FX, BioTek, Winooski, Vermont, USA).

2.3 | Microcomputed tomography

Limbs were dissected and skin removed at time of euthanasia and immediately fixed in 4% paraformaldehyde for 24–48 h. To assess morphological bone differences between *Fgf9*^{ScxCre} and WT mice, fixed limbs were wrapped in 70% ethanol-soaked gauze and scanned using microcomputed tomography (microCT; Skyscan 1276, Bruker, Belgium) with acquisition settings optimized for mouse limb imaging (0.5 mm Aluminum filter, 10.6 μm voxel size, 50 kV voltage, 200 mA current, and 950 ms exposure time, 0.3° rotation step, and 360°scan). Humeral epiphyses and calcaneal apophyses were segmented based on the growth plate morphology (humeral epiphysis: superior to the growth plate; calcaneal apophysis: posterior to the growth plate) using CTAN software (Bruker, Belgium). Tissue volume (TV), bone volume (BV), and bone volume ratio (BV/TV, %) in the calcaneus as well as the humeral and calcaneal epiphyses were measured, and for both the humerus and the calcaneus, bone length, bone mineral density (BMD), and diaphyseal cortical thickness were measured following mineral density calibration. Mineralized insertional thickness (mm) was measured manually in the mid-sagittal plane for the humeral head and calcaneus at the supraspinatus and Achilles tendon entheses, respectively, using CTAn Software (Bruker, Belgium). Thickness measurements were repeated three times along the anatomical site of the attachment for both Achilles and supraspinatus entheses. Percent variation was calculated between at least three in-plane slices to test for repeatability of measurement and values were averaged for quantitative analysis (standard error of mean <3%).

2.4 | Histology

Fixed tissues were decalcified (Formical-2000, StatLab, McKinney, TX), paraffin-embedded, and sectioned at 6 μm thickness. For staining, Toluidine Blue and Hematoxylin & Eosin (H&E) stains were used for qualitative assessment of proteoglycan and overall enthesis morphology at the Achilles and supraspinatus entheses, respectively. Additionally, sections were stained with Masson's Trichrome to assess formation of the fibrocartilaginous enthesis. Stained slides were imaged using brightfield microscopy (Imager A2 microscope, Carl Zeiss, Germany).

Enthesis cellularity was measured from Toluidine Blue-stained slides of normally developing neonatal, young-adult, and adult samples. Entheses were manually segmented based on the cellular morphology and the change in GAG distribution, using particle analysis in ImageJ software. In the adult WT and *Fgf9*^{ScxCre} attachment sites, cell nuclei were stained with DAPI. Fluorescent images were taken using the DAPI channel (20x objective, Axio Observer.Z1 microscope, Carl Zeiss, Germany). The total number of nuclei in a field of view was quantified from DAPI-stained images using a manually defined rectangular area (130 μm × 200 μm for Achilles' insertion site and 60 μm × 130 μm for Supraspinatus) at the mid-enthesis

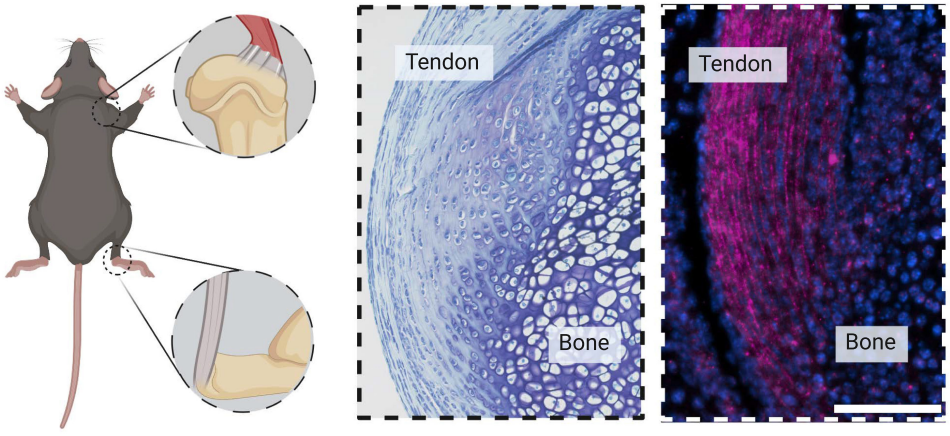

FIGURE 1 Interfaces analyzed included the supraspinatus enthesis of the mouse shoulder and the Achilles enthesis of the mouse foot (left panel). The middle and right panels, respectively, show the morphology of the developing enthesis (stained with Toluidine Blue) and expression of *Fgf9* (shown in magenta) of the neonatal Achilles' enthesis and tendon. Fluorescent in situ hybridization for Mm-*Fgf9*. Scale bar = 100 μm. Figure made using Biorender.

TABLE 1 Bone morphometric measurements at the site of Achilles and supraspinatus attachments at 8 weeks of age.

Anatomical site	WT	*Fgf9*^{ScxCre}	*p*-value
Humerus			
Length (mm)	11.76 ± 0.55	11.31 ± 0.56	.0919
Cortical thickness at mid-diaphysis (mm)	0.17 ± 0.02	0.15 ± 0.02	.2870
Cortical BMD at mid-diaphysis (g/cm^3)	0.73 ± 0.03	0.757 ± 0.04	.1295
Humeral epiphysis			
TV (mm^3)	2.42 ± 0.17	2.14 ± 0.13	.0045*
BV (mm^3)	0.95 ± 0.17	0.87 ± 0.16	.2135
BV/TV (%)	39.34 ± 6.23	40.78 ± 7.14	.3592
Trabecular TV (mm^3)	1.21 ± 0.15	1.13 ± 0.09	.1609
Trabecular BV (mm^3)	0.42 ± 0.08	0.35 ± 0.06	.0431*
Trabecular BV/TV (%)	35.22 ± 5.34	30.40 ± 4.23	.0572
Trabecular number (1/mm)	5.19 ± 0.25	4.83 ± 0.30	.0254*
Trabecular thickness (μm)	0.07 ± 0.01	0.06 ± 0.01	.1367
Trabecular separation (μm)	0.17 ± 0.02	0.17 ± 0.020	.4046
Calcaneus			
Length (mm)	3.75 ± 0.13	3.62 ± 0.12	.0431*
TV (mm^3)	2.80 ± 0.39	2.36 ± 0.31	.0175*
BV (mm^3)	2.08 ± 0.45	1.59 ± 0.37	.0239*
BV/TV (%)	73.55 ± 7.07	66.97 ± 6.69	.0495*
Cortical thickness (mm)	0.20 ± 0.04	0.17 ± 0.04	.0942
Cortical BMD (g/cm^3)	0.76 ± 0.15	0.73 ± 0.16	.6599
Calcaneal epiphysis			
TV (mm^3)	0.14 ± 0.04	0.11 ± 0.03	.0415*
BV (mm^3)	0.13 ± 0.04	0.09 ± 0.03	.0644
BV/TV (%)	84.48 ± 6.02	82.75 ± 6.82	.6241
TMD (g/cm^3)	0.63 ± 0.10	0.54 ± 0.12	.1825

Note: Mean ± standard deviation.

*$p < .05$.

region (Figure 6). Selected regions were verified by bright-field images of the insertion sites. Images were converted to grayscale, thresholded, and pre-processed. Particle analysis was subsequently performed using ImageJ software.[26]

2.5 | Immunohistochemistry

Expression of type X collagen (Col X) is an indicator of chondrocyte hypertrophy and marks the mineralization front of both the growth plate and enthesis.[3] Immunohistochemistry was used to assess the distribution of Col X, marker of the mineralization front in the ECM. Sectioned slides from Young samples were deparaffinized and rehydrated to 70% ethanol ($n >= 4$/genotype). Heat-mediated antigen retrieval was performed at 65°C (sodium citrate Buffer, pH 6.0). Slides were quenched and blocked at room temperature using 0.3% hydrogen peroxide (Santa Cruz, Dallas, TX) and 5% goat serum in PBS, respectively. Primary rabbit monoclonal anti-collagen X antibody (Abcam, ab260040; 1:100) with HRP/DAB system (Millipore Sigma) was used for detection of Col X. Slides were counterstained with hematoxylin and coverslipped with acrylic mounting media (Acrymount, Statlab, McKinney, TX, USA). The presence of Col X in the ECM was quantified at the secondary ossification center by segmentation based on cellular and tissue morphology, and the region with Col X localization was measured using ImageJ software.[26]

2.6 | Mechanical testing

For biomechanics, frozen contralateral hindlimbs were thawed overnight and calcanei were dissected with

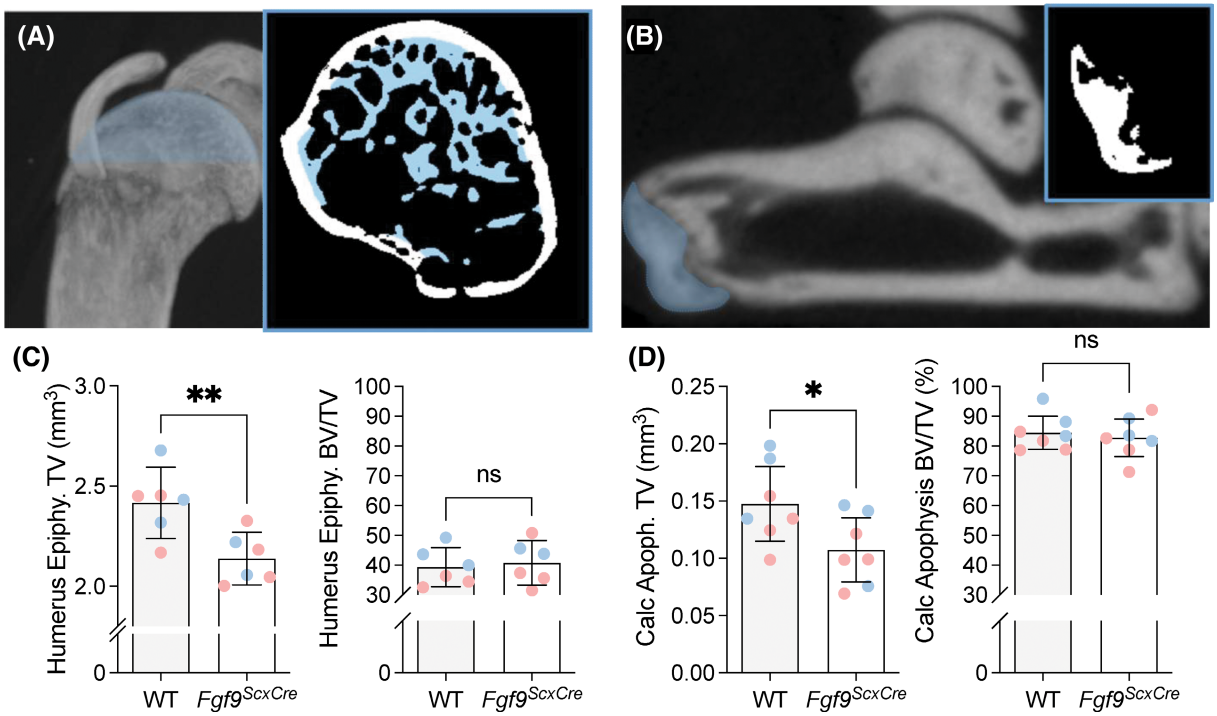

FIGURE 2 At 8 weeks of age, *Fgf9*^{ScxCre} mice had smaller humeral epiphyses and calcaneal apophyses compared to age-matched WT littermates. (A and B) Schematics showing segmentation of bone, with blue pseudo-color indicating trabecular bone and white pseudo-color indicating cortical bone, of (A) the humeral epiphysis and (B) calcaneal apophyses. (C and D) Humeral epiphyses and calcaneal apophyses were smaller in *Fgf9*^{ScxCre} mice compared to age-matched controlled but epi/apophyseal bone volume ratio (BV/TV did not differ. Blue and pink dots denote male and female mice, respectively. Data presented as mean ± 95% CI; *$p < .05$; **$p < .01$.

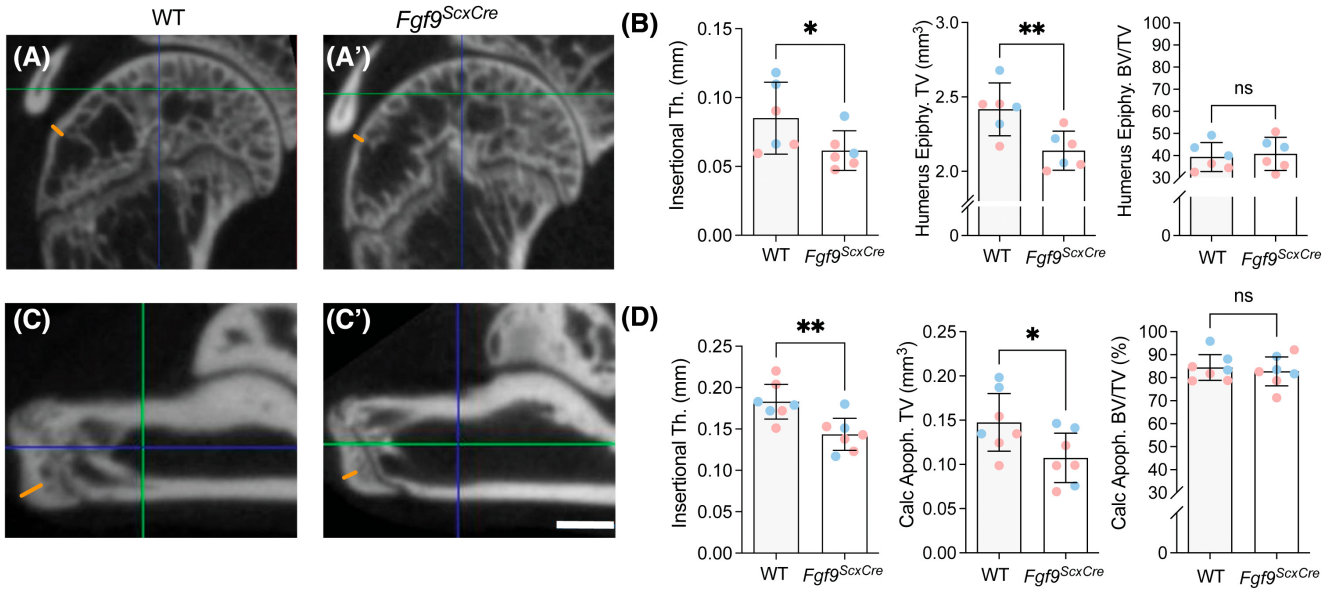

FIGURE 3 Insertional thickness in mature 8 week-old *Fgf9*^{ScxCre} entheses was significantly thinner compared to age-matched WT mice. Respective grayscale microCT images of (A and A') supraspinatus and (C and C') Achilles entheses and regions of repeated thickness measurement (blue lines) are shown. (B and D) Measured thickness was significantly thinner at the (B) supraspinatus and (D) Achilles attachments. Blue and pink dots denote male and female mice, respectively. Data presented as mean ± 95% CI and *$p < .05$; **$p < .01$. Scale bar = 600 μm.

minimal interruption of the Achilles attachment site. Bone-tendon complexes were equilibrated in PBS at room temperature prior to testing. Plantaris tendon and the gastrocnemius/soleus muscles were carefully removed without disruption of the Achilles tendon and enthesis. To avoid slip, samples were clamped in a custom-made

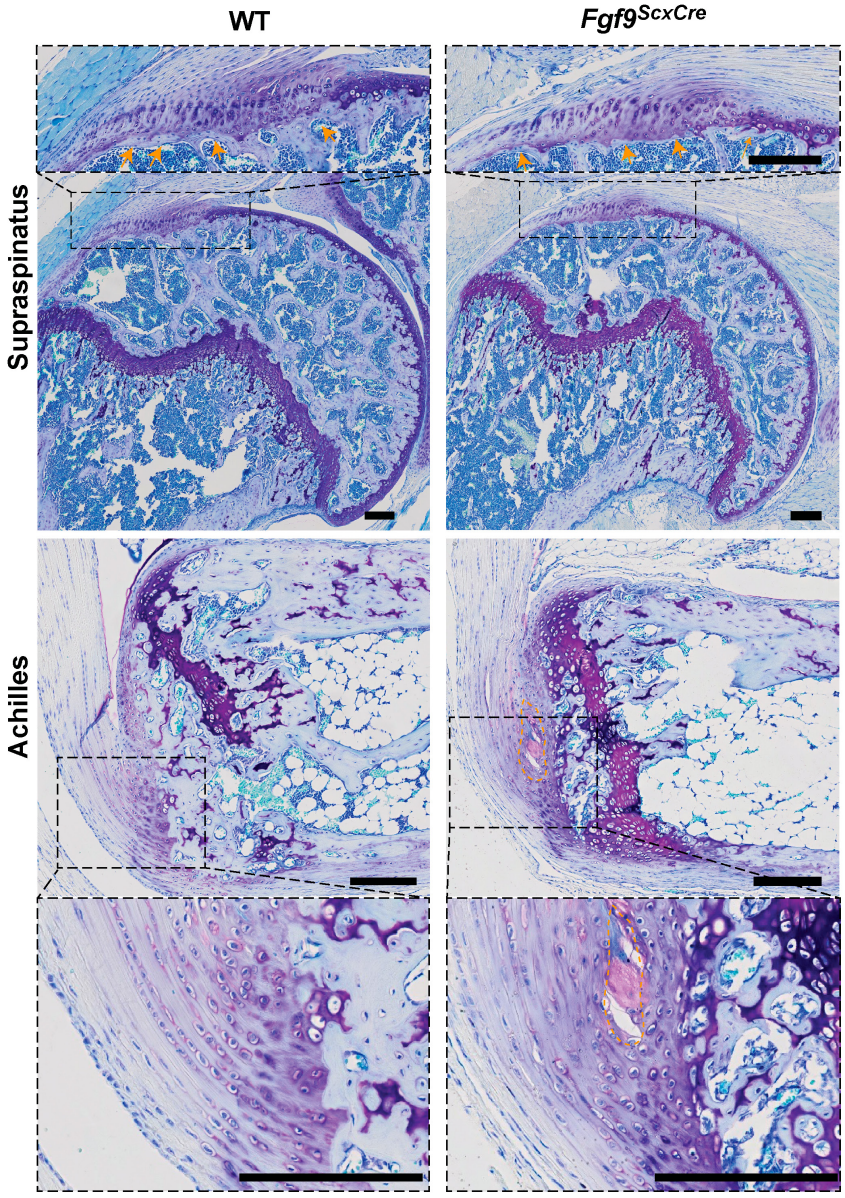

FIGURE 4 The structurally mature supraspinatus and Achilles enthesis of 8-week-old *Fgf9*^{ScxCre} mice had thinner cortical bone compared to age-matched WT mice (orange arrows), as well as smaller apophyses. *Fgf9*^{ScxCre} mice also had acellular metachromatic regions (orange dashed outline in Achilles entheses), shown in Toluidine blue stained sections of Achilles, compared to WT mice; scale bar = 100 μm scale for all panels.

fixture using sandpaper. Mechanical tests were performed using an electromechanical uniaxial tester (Instron 5943, Norwood, MA). All samples were tested in a saline bath at room temperature. For each sample, the major diameter area and gauge length were measured at 0.01 N preload using a scaled image captured on video in frame of the preloaded sample. The cross-sectional area was then calculated with the assumption of ellipsoidal geometry with a diametric ratio of 7/5. The loading protocol consisted of a ramp to 0.02 N, preconditioning with 10 cycles (0.02–0.04 N), and displacement to failure at 0.03 mm/s rate. Force–displacement data were collected and analyzed using a custom Matlab code to calculate stiffness, ultimate load, work to ultimate load, elastic modulus, ultimate stress, strain at ultimate stress, and area under the curve (i.e., toughness).

2.7 | Statistical analysis

Statistical analyses were performed using Prism (Graphpad, La Jolla, CA). Quantitative data are presented as dot plots with mean ±95% confidence interval unless otherwise indicated, and male and female mice are annotated as blue and pink dots, respectively. Data were analyzed for normality using Shapiro–Wilk test. Results from bone morphometry (microCT), nuclear and Col X quantification, and uniaxial tensile testing were compared between WT and *Fgf9*^{ScxCre} samples using two-tailed unpaired t-tests (assuming Gaussian distribution). Comparisons between mouse ages for cellularity measurements of neonatal, young-adult, and adult entheses, were performed using a one-way ANOVA and Tukey's multiple comparisons analysis.

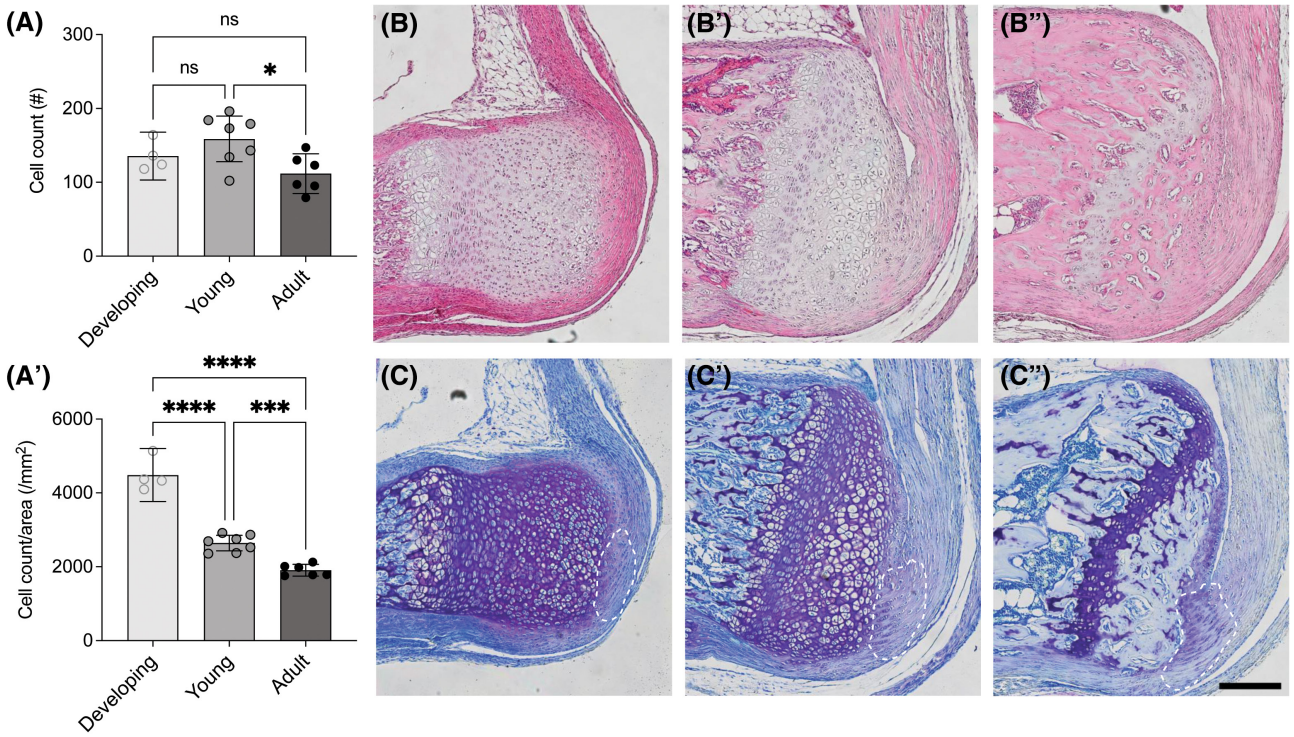

FIGURE 5 During post-natal development, the cellular density of the enthesis decreased. (A) Total cell count and (A') cell count per area (cellularity) were measured using ImageJ using the outlined regions of the enthesis (shown as white dashed areas in C). Histological representation of the Achilles enthesis stained using (B) H&E and (C) Toluidine Blue during developing stages, as well as for the (B' and C') young-adult enthesis and (B'' and C'') adult enthesis. Scale bar = 200 μm. Data presented as mean ± 95% CI; *$p < .05$; ***$p < .0007$; ****$p < .0001$.

3 | RESULTS

3.1 | *Fgf9* is expressed in the Achilles tendon and attachment and loss of *Fgf9* in tendon progenitors leads to impaired apophyseal and entheseal growth

Fgf9 is robustly expressed postnatally (postnatal day 0) in the neonatal enthesis and tendon (Figure 1). At 8 weeks of age, the enthesis is considered structurally mature in normally developed mice. This also translates to maturation of the secondary ossification centers (e.g., epiphysis of the proximal humerus and calcaneal apophysis) followed later by closure of the primary growth plates. In mice with FGF9 deletion in the tendon progenitors throughout embryonic and postnatal growth (using ScxCre), we observed both reduced trabecular bone volume and trabecular number at the humeral epiphysis compared to age-matched WT controls, as measured using microCT (Table 1). The calcaneus of $Fgf9^{ScxCre}$ mice was significantly shorter and had reduced bone and tissue volume compared to WT (Table 1). $Fgf9^{ScxCre}$ mice had lower tissue volume in the adult humeral and calcaneal epiphyses (Figure 2) and thinner subchondral bone thickness at supraspinatus and Achilles' tendon attachments at the humeral head and posterior calcaneus, respectively (Figure 3).

Cortical thinning at the supraspinatus and Achilles entheses in mature $Fgf9^{ScxCre}$ attachments was confirmed using histology (Figure 4). $Fgf9^{ScxCre}$ mice developed an acellular metachromatic region at the superior Achilles enthesis which was not present in WT mice (Figure 4).

3.2 | *Fgf9* deletion in the tendon progenitors resulted in increased cellularity and delayed maturation of the enthesis

During normal postnatal growth, the developing enthesis and secondary ossification (Figure 5B,C) begins mineralizing at 2 to 4 weeks of age (Figure 5B',C') and continues to mature until the gradient fibrocartilage with subchondral bone and mineralized/unmineralized fibrocartilage are formed by 8 weeks of age (Figure 5B'',C''). Histological assessment showed that the area of the Achilles enthesis increased from developing ($0.03 \pm 0.003\,mm^2$) to young-adult samples ($0.06 \pm 0.014\,mm^2$) (Figure 5). Cellular

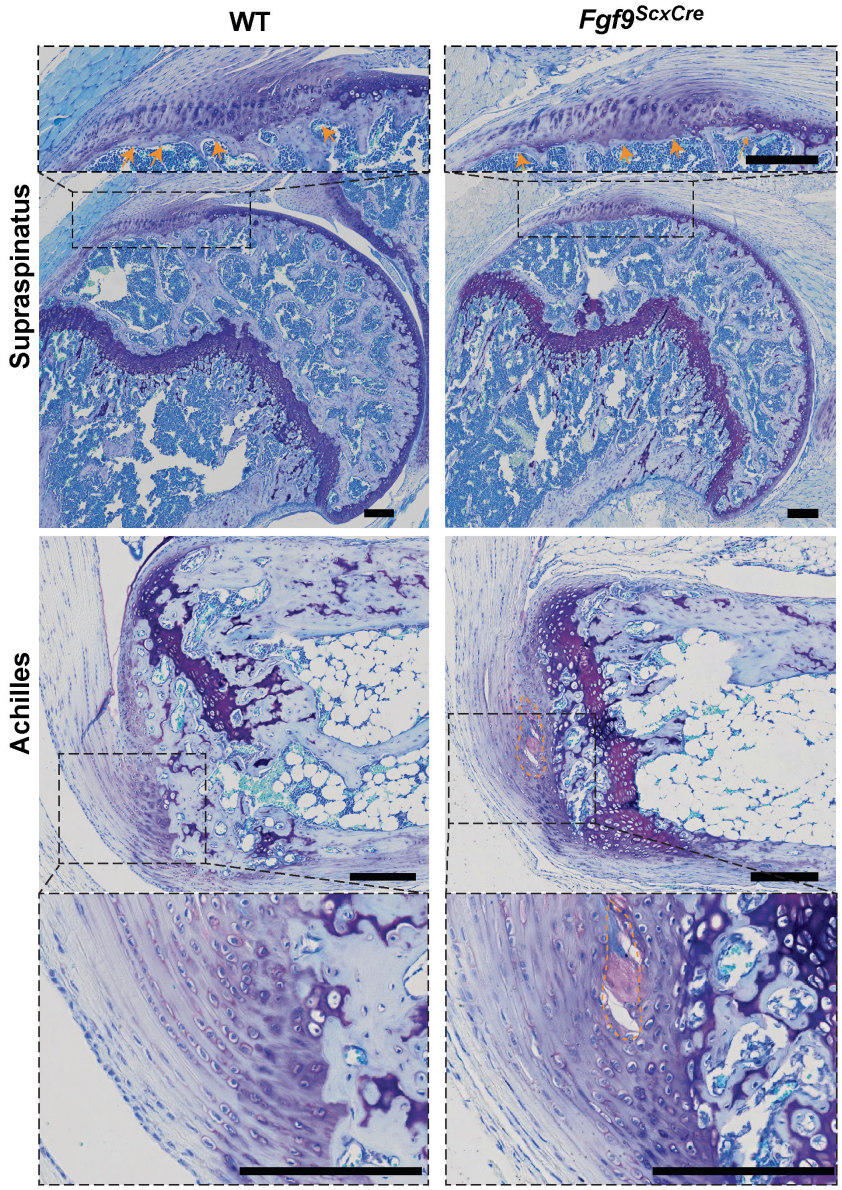

FIGURE 6 Cellular density was higher in mature supraspinatus entheses of 8-week-old $Fgf9^{ScxCre}$ mice compared to WT. (A) Representative fluorescent images of supraspinatus and Achilles' regions of interest (scale bar 20 μm). (B) Nuclear density and (C) number of nuclei presented for both $Fgf9^{ScxCre}$ and WT mice at 8 weeks of age; Pink dots/lines = female mice; Blue dots/lines = male mice. Scale bar = 50 μm. Data presented as mean ± 95% CI and $p < .05$.

density of the enthesis also decreased during postnatal development (Developing vs. Young-adult: $p < .0001$; Developing vs. Adult: $p < .0001$; Young-adult vs. Adult: $p = .0007$) (Figure 5A'). In $Fgf9^{ScxCre}$ mice, cellular density of adult entheses at 8 weeks of age was higher at the supraspinatus ($p < .01$) and Achilles ($p = .0563$) tendon attachment sites compared to WT mice (Figure 6).

3.3 | Tendon/enthesis-specific deletion of *Fgf9* led to impaired enthesis mechanical properties

Achilles tendon entheses of $Fgf9^{ScxCre}$ mice had reduced ultimate load at 8 weeks of age ($p = .0406$, Figure 7A,C) with no change in cross-sectional area (CSA; Figure 7B, $p = .77$), stiffness ($p = .1415$, Table 2), or work to max load ($p = .1126$, Table 2). Tensile mechanical properties did not change between $Fgf9^{ScxCre}$ and WT tendon entheses (elastic modulus: $p = .6451$, Table 2; maximum stress: $p = .1701$, Table 2; strain at max stress: $p = .3175$, Table 2; or toughness: $p = .1241$, Table 2).

3.4 | Loss of *Fgf9* in enthesis progenitors resulted in delayed mineralization

To investigate the underlying changes associated with structural adaptation in adult enthesis, the mineralization of the secondary ossification center (SOC) was characterized at 3 weeks of age (i.e., during enthesis mineralization) using Masson's Trichrome staining and immunohistochemistry (IHC) for type X collagen (Col

X). Young *Fgf9*^{ScxCre} calcanei had fewer hypertrophic chondrocytes at the SOC compared to WT (Figure 8A,B). Interestingly, while the size of the SOC did not significantly differ between groups ($p = .1972$, Figure 8C), the Col X+ area within the SOC was smaller in *Fgf9*^{ScxCre} mice compared to WT mice at 3 weeks of age ($p = .035$; Figure 8D–F).

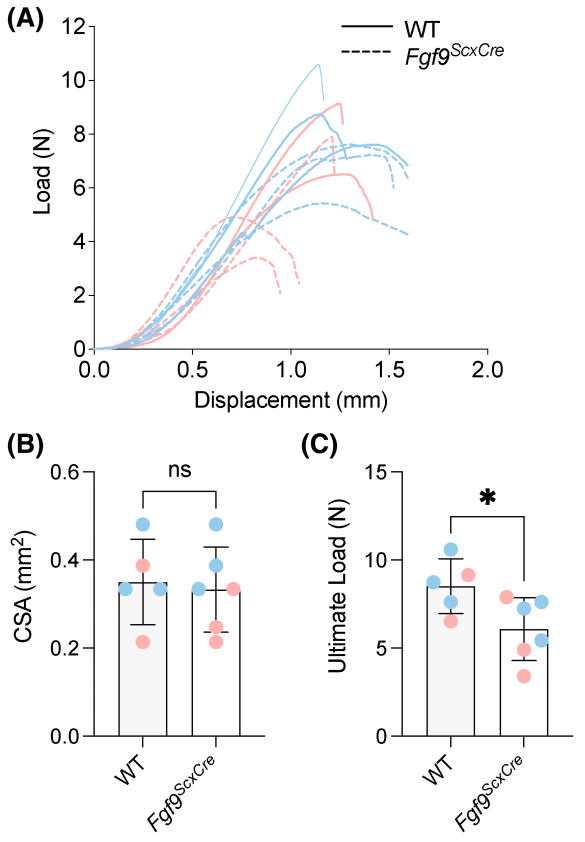

FIGURE 7 Targeted *Fgf9* deletion disrupts tensile mechanics of mature Achilles enthesis. Achilles tendon enthesis of 8-week-old *Fgf9*^{ScxCre} mice had reduced ultimate load compared to age-matched WT mice. (A) Overlaid load–displacement curves, (B) CSA, and (C) maximum load for all samples tested. Pink dots/lines = female mice; Blue dots/lines = male mice. Error bars denote mean ± 95% CI, *$p < .05$; ns = not significantly different.

4 | DISCUSSION

In this study, we investigated the role of tendon/enthesis-derived Fgf9 on the postnatal maturation of two functionally graded fibrocartilaginous entheses (i.e., Achilles and supraspinatus). We showed that, unlike the growth plate,[27] *Fgf9* is expressed postnatally in tendon and enthesis. We then showed that constitutive deletion of *Fgf9* using ScxCre led to smaller but more cellular mature tendon interfaces with fewer hypertrophic chondrocytes and less Col X+ matrix in the young (i.e., maturing) apophysis. This suggests a potent disruption and delay in endochondral-like bone formation driven by loss of *Fgf9* in the enthesis and SOC, similar to findings from growth plates of global *Fgf9*$^{-/-}$ mutants.[15] These mineralization delays may have contributed to the lower biomechanical properties (e.g., ultimate load) of the mature tendon enthesis.

Others have also shown that disruption of the mineral matrix can significantly reduce the tensile strength of the enthesis.[28,29] Surprisingly, despite the thinner mineral thickness at the adult supraspinatus and Achilles entheses, *Fgf9*^{ScxCre} mice had increased cellular density at the attachment site. Previously, increased mesenchymal cellularity has been linked to the delayed palatal growth in embryos with global deletion of *Fgf9*.[30] Thus, the increased cellularity in the mature enthesis we observed is likely due to delayed maturation in the *Fgf9*^{ScxCre} enthesis that is also evident by smaller area of active matrix mineralization in the young enthesis. Additionally, the acellular metachromatic defect at the Achilles enthesis of *Fgf9*^{ScxCre} mice may indicate an altered microenvironment at the tendon-bone attachment, caused by changes in compressive loading of the tendon that results in increased proteoglycan formation.[31–33] Lastly, a potential explanation for the reduced bone morphometric properties may be linked to decreased effective load transfer through the supraspinatus enthesis that manifests from decreased remodeling and mineral deposition near the enthesis.[34,35]

TABLE 2 Descriptive and comparative uniaxial tensile test results for Achilles tendons/entheses in WT and Fgf9^{ScxCre} at 8 weeks of age.

	WT	*Fgf9*^{ScxCre}	*p*-value
Stiffness (N/mm)	11.23 ± 2.11	9.088 ± 2.26	.1415
Ultimate load (N)	8.52 ± 1.55	0	.0406*
Work to ultimate load (mJ)	4.56 ± 0.57	3.26 ± 1.55	.1126
Elastic modulus (MPa)	138.4 ± 37.7	124.2 ± 57.0	.6451
Maximum stress (MPa)	25.36 ± 5.67	19.31 ± 7.42	.1701
Strain at max stress (mm/mm)	0.298 ± 0.03	0.265 ± 0.67	.3175
Toughness (MJ/mm^3)	3.37 ± 0.92	2.39 ± 0.98	.1241

Note: Mean ± standard deviation.

*$p < 0.05$.

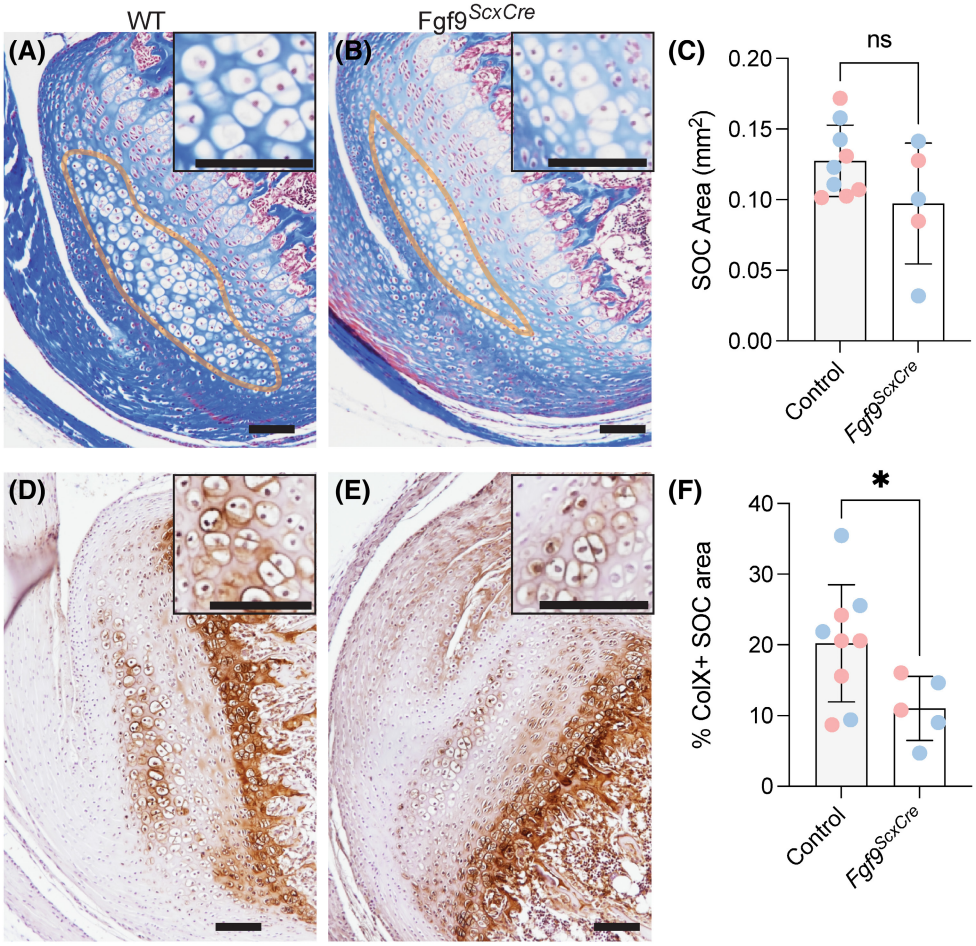

FIGURE 8 Loss of *Fgf9* in tendon and enthesis leads to reduced area of active mineralization at the SOC of the young mice at 3 weeks of age. (A and B) 3-week-old $Fgf9^{ScxCre}$ mice had smaller hypertrophic chondrocytes, however (C) the secondary ossification center (SOC) was not significantly smaller compared to age-matched WT mice. Additionally, (D–F) the size of the ColX area in the SOC was smaller in $Fgf9^{ScxCre}$ mice compared to age-matched WT littermates. *$p < .05$; ns = not significantly different ($p > .05$). Scale bars = 100 μm.

FGF9 plays a major role in vascularization of many tissues, including bone during development[15] and in muscle with reperfusion following ischemia.[36] The fibrocartilage entheses investigated in the present study are not considered well-vascularized tissues, yet the potential delays in maturation we observed may still be caused by delays in vascularization especially to the SOC.[37] Additionally, others have reported that loss of *Fgf9* during growth leads to delayed vascular invasion and, consequently, delayed initiation of chondrocyte hypertrophy,[15] which we also observed in the SOC of $Fgf9^{ScxCre}$ mice. Future studies should explore the role of FGF9 and vascularization during development of the fibrocartilaginous enthesis.[38]

This study is not without limitations. While we focused primarily on the role of FGF9 in structure and function of fibrocartilage entheses, we did not investigate migratory or fibrous entheses, like the deltoid tuberosity or the medial collateral ligament, respectively. The resident progenitor cells in these other types of entheses have more dynamic turnover during growth[39] and may offer a different perspective on FGF signaling during enthesis growth. Additionally, use of inducible Cre drivers, such as Gli1-CreERT2[40] or Scx-CreERT2[41] would reduce the potential off-target effects of *Fgf9* knockout in cartilage and perichondrium, as the constitutive ScxCre also targets chondrogenic progenitors and other cell types.

AUTHOR CONTRIBUTIONS

Elahe Ganji, David M. Ornitz, and Megan L. Killian conceived of the study; Elahe Ganji and Megan L. Killian drafted the manuscript; Elahe Ganji, David M. Ornitz, and Megan L. Killian designed the experiments; David M. Ornitz, and Megan L. Killian developed mouse models; Elahe Ganji, Connor Leek, William Duncan, Debabrata Patra, and Megan L. Killian performed research; Elahe Ganji, Connor Leek, William Duncan, Debabrata Patra, David M. Ornitz, and Megan L. Killian, wrote, edited, and approved the final manuscript.

ACKNOWLEDGMENTS

The authors thank Dr. Gwen Talham and Frank Warren for assistance with animal care at the University of Delaware and Zachary Tata for assistance with animal care at the University of Michigan. Funding for this work was provided by the National Institutes of Health (K12HD073945, R01AR079367, R03HD094594, R01HD049808, P30GM103333, P30AR069620); the National Science Foundation (1944448); the University of Delaware Research Foundation (16A01396); and the University of Delaware Doctoral Fellowship.

DISCLOSURES

The authors have stated explicitly that there are no conflicts of interest in connection with this article.

DATA AVAILABILITY STATEMENT

The data that support the findings of this study are available in the methods and/or supplementary material of this article.

ORCID

David M. Ornitz https://orcid.org/0000-0003-1592-7629
Megan L. Killian https://orcid.org/0000-0001-6868-5550

REFERENCES

1. Blitz E, Viukov S, Sharir A, et al. Bone ridge patterning during musculoskeletal assembly is mediated through SCX regulation of Bmp4 at the tendon-skeleton junction. *Dev Cell*. 2009;17(6):861-873.
2. Zelzer E, Blitz E, Killian ML, Thomopoulos S. Tendon-to-bone attachment: from development to maturity. *Birth Defects Research Part C Embryo Today*. 2014;102(1):101-112.
3. Galatz L, Rothermich S, VanderPloeg K, Petersen B, Sandell L, Thomopoulos S. Development of the supraspinatus tendon-to-bone insertion: localized expression of extracellular matrix and growth factor genes. *J Orthop Res*. 2007;25(12):1621-1628.
4. Thomopoulos S, Genin GM, Galatz LM. The development and morphogenesis of the tendon-to-bone insertion—what development can teach us about healing. *J Musculoskelet Neuronal Interact*. 2010;10(1):35-45.
5. Blitz E, Sharir A, Akiyama H, Zelzer E. Tendon-bone attachment unit is formed modularly by a distinct pool of Scx - and Sox9 -positive progenitors. *Development*. 2013;140(13):2680-2690.
6. Milz S, Rufai A, Buettner A, Putz R, Ralphs JR, Benjamin M. Three-dimensional reconstructions of the Achilles tendon insertion in man. *J Anat*. 2002;200(2):145-152.
7. Schwartz AG, Pasteris JD, Genin GM, Daulton TL, Thomopoulos S. Mineral distributions at the developing tendon enthesis. *PLoS ONE*. 2012;7(11):e48630.
8. Leek CC, Soulas JM, Bhattacharya I, et al. Deletion of fibroblast growth factor 9 globally and in skeletal muscle results in enlarged tuberosities at sites of deltoid tendon attachments. *Dev Dyn*. 2021;250(12):1778-1796.
9. Roberts RR, Bobzin L, Teng CS, et al. FGF signaling patterns cell fate at the interface between tendon and bone. *Development*. 2019;146:dev170241.
10. Su N, Jin M, Chen L. Role of FGF/FGFR signaling in skeletal development and homeostasis: learning from mouse models. *Bone Res*. 2014;2:1-24.
11. Hung IH, Schoenwolf GC, Lewandoski M, Ornitz DM. A combined series of Fgf9 and Fgf18 mutant alleles identifies unique and redundant roles in skeletal development. *Dev Biol*. 2016;411(1):72-84.
12. Charoenlarp P, Rajendran AK, Iseki S. Role of fibroblast growth factors in bone regeneration. *Inflamm Regen*. 2017;37:10.
13. Naski MC, Ornitz DM. FGF signaling in skeletal development. *Pediatr Pathol Mol Med*. 1998;18(4–5):355-379.
14. Ornitz DM, Marie PJ. FGF signaling pathways in endochondral and intramembranous bone development and human genetic disease. *Genes Dev*. 2002;16(12):1446-1465.
15. Hung IH, Yu K, Lavine KJ, Ornitz DM. FGF9 regulates early hypertrophic chondrocyte differentiation and skeletal vascularization in the developing stylopod. *Dev Biol*. 2007;307(2):300-313.
16. Behr B, Leucht P, Longaker MT, Quarto N. Fgf-9 is required for angiogenesis and osteogenesis in long bone repair. *Proc Natl Acad Sci U S A*. 2010;107(26):11853-11858.
17. Garofalo S, Kliger-Spatz M, Cooke JL, et al. Skeletal dysplasia and defective chondrocyte differentiation by targeted overexpression of fibroblast growth factor 9 in transgenic mice. *J Bone Miner Res*. 1999;14(11):1909-1915.
18. Karuppaiah K, Yu K, Lim J, et al. FGF signaling in the osteoprogenitor lineage non-autonomously regulates postnatal chondrocyte proliferation and skeletal growth. *Development*. 2016;143(10):1811-1822.
19. Schweitzer R, Chyung JH, Murtaugh LC, et al. Analysis of the tendon cell fate using Scleraxis, a specific marker for tendons and ligaments. *Development*. 2001;128(19):3855-3866.
20. Brent AE, Braun T, Tabin CJ. Genetic analysis of interactions between the somitic muscle, cartilage and tendon cell lineages during mouse development. *Development*. 2005;132(3):515-528.
21. Asou Y, Nifuji A, Tsuji K, et al. Coordinated expression ofscleraxis andSox9 genes during embryonic development of tendons and cartilage. *J Orthop Res*. 2002;20(4):827-833.
22. Shukunami C, Takimoto A, Nishizaki Y, et al. Scleraxis is a transcriptional activator that regulates the expression of Tenomodulin, a marker of mature tenocytes and ligamentocytes. *Sci Rep*. 2018;8(1):3155.
23. Killian ML, Thomopoulos S. Scleraxis is required for the development of a functional tendon enthesis. *FASEB J*. 2016;30(1):301-311.
24. Sugimoto Y, Takimoto A, Hiraki Y, Shukunami C. Generation and characterization of ScxCre transgenic mice. *Genesis*. 2013;51(4):275-283.
25. Sugimoto Y, Takimoto A, Akiyama H, et al. Scx+/Scx9+ progenitors contribute to the establishment of the junction between cartilage and tendon/ligament. *Development*. 2013;140(11):2280-2288.
26. Schneider CA, Rasband WS, Eliceiri KW. NIH image to ImageJ: 25 years of image analysis. *Nat Methods*. 2012;9(7):671-675.
27. Lazarus JE, Hegde A, Andrade AC, Nilsson O, Baron J. Fibroblast growth factor expression in the postnatal growth plate. *Bone*. 2007;40(3):577-586.
28. Golman M, Abraham AC, Kurtaliaj I, et al. Toughening mechanisms for the attachment of architectured materials: the mechanics of the tendon enthesis. *Sci Adv*. 2021;7(48):eabi5584.

29. Schwartz A, Lipner J, Pasteris J, et al. Muscle loading is necessary for the formation of a functional tendon enthesis. *Bone*. 2013;55(1):44-51.
30. Li R, Sun Y, Chen Z, et al. The fibroblast growth factor 9 (Fgf9) participates in palatogenesis by promoting palatal growth and elevation. *Front Physiol*. 2021;12:653040.
31. Vogel KG, Ördög A, Pogány G, Oláh J. Proteoglycans in the compressed region of human tibialis posterior tendon and in ligaments. *J Orthop Res*. 1993;11(1):68-77.
32. Vogel KG. The effect of compressive loading on proteoglycan turnover in cultured fetal tendon. *Connect Tissue Res*. 1996;34(3):227-237.
33. Yoon JH, Halper J. Tendon proteoglycans: biochemistry and function. *J Musculoskelet Neuronal Interact*. 2005;5(1):22-34.
34. Mullender MG, Huiskes R. Proposal for the regulatory mechanism of Wolff's law. *J Orthop Res*. 1995;13(4):503-512.
35. Biewener AA, Fazzalari NL, Konieczynski DD, Baudinette RV. Adaptive changes in trabecular architecture in relation to functional strain patterns and disuse. *Bone*. 1996;19(1):1-8.
36. Said SS, Yin H, Elfarnawany M, et al. Fortifying angiogenesis in ischemic muscle with FGF9-loaded electrospun poly(ester amide) fibers. *Adv Healthc Mater*. 2019;8(8):1801294.
37. Gao J, Messner K, Ralphs JR, Benjamin M. An immunohistochemical study of enthesis development in the medial collateral ligament of the rat knee joint. *Anat Embryol*. 1996;194(4):399-406.
38. Maes C, Carmeliet P, Moermans K, et al. Impaired angiogenesis and endochondral bone formation in mice lacking the vascular endothelial growth factor isoforms VEGF164 and VEGF188. *Mech Dev*. 2002;111(1–2):61-73.
39. Felsenthal N, Rubin S, Stern T, et al. Development of migrating tendon-bone attachments involves replacement of progenitor populations. *Development*. 2018;145:dev165381.
40. Ahn S, Joyner AL. Dynamic changes in the response of cells to positive hedgehog signaling during mouse limb patterning. *Cell*. 2004;118(4):505-516.
41. Howell K, Chien C, Bell R, et al. Novel model of tendon regeneration reveals distinct cell mechanisms underlying regenerative and fibrotic tendon healing. *Sci Rep*. 2017;7(1):45238.

How to cite this article: Ganji E, Leek C, Duncan W, Patra D, Ornitz DM, Killian ML. Targeted deletion of *Fgf9* in tendon disrupts mineralization of the developing enthesis. *The FASEB Journal*. 2023;37:e22777. doi:10.1096/fj.202201614R